ENGINEERING

Poro-elasto-capillary wicking of cellulose sponges

Jonghyun Ha,[1] Jungchul Kim,[2] Yeonsu Jung,[1] Giseok Yun,[1] Do-Nyun Kim,[1] Ho-Young Kim[1]*

We mundanely observe cellulose (kitchen) sponges swell while absorbing water. Fluid flows in deformable porous media, such as soils and hydrogels, are classically described on the basis of the theories of Darcy and poroelasticity, where the expansion of media arises due to increased pore pressure. However, the situation is qualitatively different in cellulosic porous materials like sponges because the pore expansion is driven by wetting of the surrounding cellulose walls rather than by increase of the internal pore pressure. We address a seemingly so simple but hitherto unanswered question of how fast water wicks into the swelling sponge. Our experiments uncover a power law of the wicking height versus time distinct from that for nonswelling materials. The observation using environmental scanning electron microscopy reveals the coalescence of microscale wall pores with wetting, which allows us to build a mathematical model for pore size evolution and the consequent wicking dynamics. Our study sheds light on the physics of water absorption in hygroscopically responsive multiscale porous materials, which have far more implications than everyday activities (for example, cleaning, writing, and painting) carried out with cellulosic materials (paper and sponge), including absorbent hygiene products, biomedical cell cultures, building safety, and cooking.

INTRODUCTION

As a major constituent of plants, cellulose has been used as a source of energy ([1]), food ([2], [3]), building materials ([4], [5]), clothing ([6]), and hygiene products ([7]) throughout human history. In particular, transfer and preservation of information has relied on wetting of cellulosic materials for millennia, beginning with papyrus in 3000 BCE. Porous materials made of cellulose still abound around us as paper and sponges, among many others ([8], [9]). When we bring a dry paper or sponge into contact with water or ink, it absorbs the liquid while swelling simultaneously. Cellulose is a polymer whose chains are linked via a hydrogen bonding, and water molecules participate in the binding sites, causing the polymer volume to increase. Such physicochemical interaction of water and porous structure is called hygroscopic expansion, a mundane process observed in cleaning ([10]), painting ([11]), and writing ([12]).

Capillary imbibition of liquid in porous media ([12]–[15]) is described by Darcy's law, which gives the flow rate, $\mathbf{q}$, as a function of the permeability k and gradient of driving pressure ∇p: $\mathbf{q} = -(k/\mu)\nabla p$, where μ is the liquid viscosity. Because the permeability and the driving capillary pressure are respectively scaled as the cross-sectional area of the fluid conduit and the meniscus curvature at the wetting front, both of them are determined by the pore size. When the porous structure deforms due to liquid infiltration, the poroelastic theory gives the pore size and the flow rate in general. The theory is built upon the basic assumption that the pore pressure increases with the water content, the amount of liquid inside the void, which in turn causes the pore to swell ([16]). It has successfully described the behavior of liquids in many porous media, such as soil ([17]), sandstone ([18]), and hydrogel ([19]). However, the present problem of wicking and hygroexpansion defies such classical theoretical understanding for the following reason. As water progressively wets the cellulose materials, the macroscale pores at the spreading front expand due to swelling of the surrounding walls or scaffolds, not by increased pore pressure. The pore pressure should rather decrease because of volume expansion. This disobeys the fundamental framework of poroelastic theory, and thus, a completely different approach should be devised to understand the hygroscopic expansion of cellulosic porous materials containing macro voids.

[1]Department of Mechanical and Aerospace Engineering, Seoul National University, Seoul 08826, Korea. [2]Department of Extreme Thermal Systems, Korea Institute of Machinery and Materials, Daejeon 34103, Korea.
*Corresponding author: hyk@snu.ac.kr

RESULTS

Characteristics of cellulose sponges

As a model system to study this problem, we bring a commercial cellulose sponge (VWR) into contact with water or various liquids (table S1) and observe the liquid front rise against gravity (Fig. 1A). When using aqueous liquids, the sponge swells while being wetted. Plotting the rise height h versus time t (Fig. 1B) reveals that the power laws of h versus t differ in the early (filled symbols) and late (empty symbols) stages. Here, the heights are scaled by h_J, Jurin's height ([20]), a characteristic rise height at which the gravitational and capillary forces for a macropore are balanced: $h_J = \gamma/(\rho g R)$, with γ, ρ, and g being the liquid-air surface tension coefficient, the liquid density, and the gravitational acceleration, respectively. Figure 1C shows that the transition height at which the power law changes from $h \sim t^{1/2}$ (filled symbols) to $h \sim t^{1/5}$ (empty symbols) corresponds to Jurin's height of macro voids. Rationalizing these power laws allows us to understand the fundamental wicking dynamics of the hygroexpansive, heterogeneous porous materials.

We begin with characterizing the pore structure of the cellulose sponge. As shown in the scanning electron microscopy (SEM) images (Fig. 2, A to C), it consists of numerous cellulose sheets with two-dimensional microscale pores surrounding macro voids ([13]). The sheets approximately 10 nm in thickness are randomly stacked with nanometric spacings. Measuring the size distribution of the pores, we find the average radii of macro and micro voids to be $R = 0.73$ mm and $r_0 = 4$ μm, respectively (fig. S1). Pores finer than the micrometric voids are hardly found in the sheets.

Capillary flows and volumetric expansion in porous media

Darcy's law gives the wicking velocity u in a porous medium, which we now write as $u = -(k/\mu)dp/dz$. The driving pressure arises as a consequence of capillary action so that $\Delta p \sim \gamma/\lambda$, where $\sim$ signifies "is scaled as" and λ is the radius of curvature of the front meniscus. The permeability k is scaled as the cross-sectional area of fluid conduit, over which the viscous stress resisting the fluid flow develops. Noting that h measures the distance from the free surface of the liquid reservoir to the wet front, u and $\dot{h} = dh/dt$ can differ when the media volume changes. For the isotropically expanding materials like cellulose sponges as shown in Fig. 3D, the bottom of the sponge descends by $h\varepsilon_s$, with ε_s being the hygroscopic strain of the saturated sponge, so that the total wet distance $H \approx h(1 + \varepsilon_s)$. Not all the liquid flowing
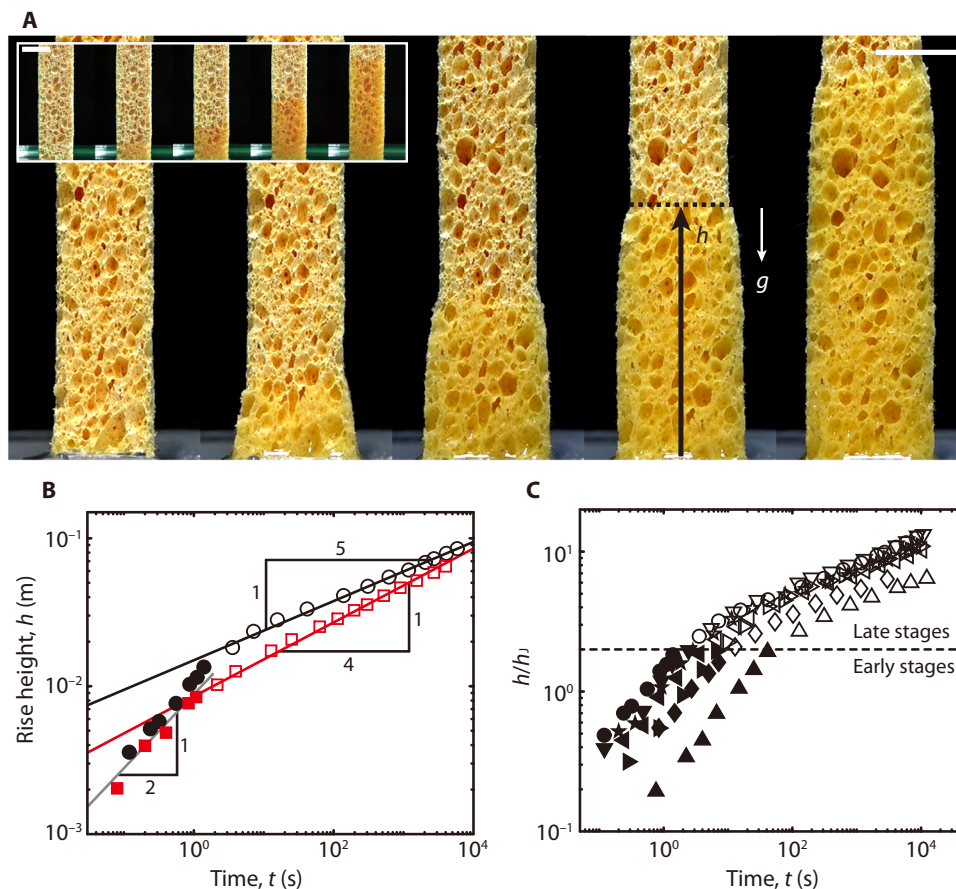
Fig. 1. Capillary rise in cellulose sponges. (**A**) Optical images for wicking of water (main panel) and turpentine (inset) in the initially dry sponge. The sponge swells when contacting water or aqueous liquids (movie S1). From left to right, t = 0, 1, 10, 100, 1000 s. Scale bar, 10 mm. (**B**) Experimentally measured rise height of water (black symbols) and turpentine (red symbols) versus time. In the early stages (filled symbols), the rise height grows like $t^{1/2}$ (gray line) for both the liquids. In the late stages (open symbols), the rise height of water follows the $t^{1/5}$ rule (black line), whereas that of turpentine behaves like $t^{1/4}$ (red line). (**C**) The power law of the height changes when the rise height h reaches Jurin's height of macropores: $h_J = \gamma/(\rho g R)$, so the transition occurs at $h/h_J \sim 1$. The symbols for different liquids are listed in table S1. All the experimental data for the rise height are the average of three measurements, with the error bars smaller than the size of symbols.

into the sponge contributes to the rise of H because of the transverse expansion of the sponge, leading us to write $\dot{H} \approx u/(1 + \varepsilon_s)^2$ (section S1). The hygroscopic strain of the used sponge is at most 0.23, allowing us to neglect higher-order terms of ε_s. Because $h \approx H/(1 + \varepsilon_s)$, we get $\dot{h} \approx u/\zeta$, with $\zeta \approx 1 + 3\varepsilon_s$ being the coefficient of volumetric expansion.

When the macro voids are completely filled with infiltrating liquid, as observed for the early stages of capillary rise (Fig. 3, A and C), $\lambda \sim R$ and $k \sim R^2$. Then, we get $\dot{h} \sim \gamma R/(\zeta \mu h)$ so that $h \sim [\gamma R t/(\zeta \mu)]^{1/2}$, which is consistent with Lucas-Washburn's rule (21, 22) except the fact that the effect of swelling (ζ) is included. We plot the rise heights of Fig. 4A according to our scaling law to find the scattered data to collapse onto a single straight line in Fig. 4B together with the data of nonaqueous liquids ($\varepsilon_s = 0$). When plotting h versus $\gamma R t/\mu$ without ζ in Fig. 4C, we find two distinct lines depending on whether the sponge swells or not.

Darcy's law for late stages
Beyond Jurin's height, macro voids cannot be completely filled because the capillary pressure based on the void radius cannot withstand the hydrostatic pressure. Then, the foregoing model fails (13), which is consistent with the change of the slopes in Fig. 1B. In this regime, the rise is rather driven by the capillary pressure provided by the micropores of characteristic radius r so that $\lambda \sim r$. However, the liquid does not flow

only through microporous sheets, but it can also wet the corners of macro voids in such a way that the radius of corner meniscus δ balances capillary and hydrostatic pressure: $\gamma/\delta \sim \rho g h$. We display the image of the macro void partially filled with liquid and its schematic in Fig. 3 (A and B). Because the liquid that advances the wetting front can be supplied from the wet corners rather than the network of micropores owing to reduced viscous stress (for $\delta \gg r$) as shown in the box of Fig. 3D, we should take the permeability k as the cross-sectional area of the wet corner. A simple geometric consideration allows us to write the area as δ^2 so that $k \sim \delta^2$. Then, Darcy's law, $u \sim \delta^2 \gamma/(\mu r h)$, gives

$$u \sim \frac{\gamma^3}{\mu(\rho g)^2 r h^3} \tag{1}$$

Pore growth due to hygroscopic swelling
When the micropore size is invariant as $r = r_0$, we easily get $h \sim t^{1/4}$, which was shown to hold for the rise of nonaqueous liquids without causing hygroscopic swelling (13). However, in case of water wicking, we have discovered drastic shape changes of micropores in an environmental SEM (ESEM) chamber, where the RH around a sponge specimen has increased from 10 to 100%. See Fig. 2D and
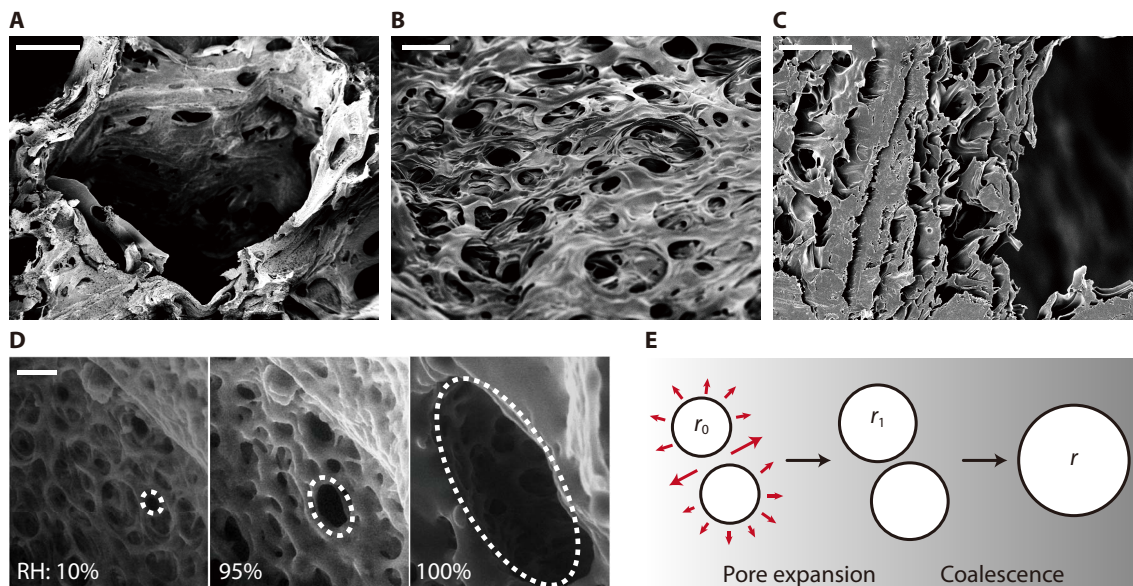
Fig. 2. Microscopic images of the cellulose sponge. SEM images of macropores (**A**), micropores (**B**), and cross section of the sheets (**C**). Scale bars, 300 μm (A) and 10 μm (B and C). (**D**) Merging of micropores due to hygroscopic expansion of the cellulose sheet, as imaged by ESEM. The pores start to grow when the relative humidity (RH) exceeds 90%, and they coalesce with their neighbors. Scale bar, 10 μm. (**E**) Schematic illustration of micropore expansion and coalescence. The micropores grow from r_0 to r_1 in radius (pore expansion) and then merge to form large micropores of radius r (coalescence).

movie S2 for experimental images and Materials and Methods for experimental procedure. The expansion process of the porous sheet can be decomposed into two steps (Fig. 2E). First, the pore size grows from r_0 to r_1, allowing us to write $r_1 \sim r_0(1 + \varepsilon)$. As the expanded pores get closer, they merge to form large pores of radius r accompanied by the decrease of the number of pores from N_0 to N. Because of the insignificant change of the total area of pores upon coalescence, we get $N_0 r_1^2 \sim N r^2$. Similar growth and coalescence of pores can be easily observed by stretching a macroscopic perforated polymer film as well as in microscopic ductile fracture (23) and polymer crack (24). The ratio $N_0/N > 1$ should increase with ε, which we simply estimate as $N_0/N \sim 1 + \beta\varepsilon$ (section S2 and figs. S1 to S4). The prefactor β is a function of a distribution of interpore distances, and a detailed discussion of the estimate is given in section S2. With the measured values of $\beta \approx 50$ and $\varepsilon \sim \varepsilon_s \approx 0.23$ in the cellulose sponges, we obtain $N_0/N \sim \beta\varepsilon$, and thus, $r \sim (\beta\varepsilon)^{1/2} r_0$. When the wet sponges are dried, a similar size distribution of micropores to the originally dry state is recovered (section S3 and fig. S5).

Hygroscopic swelling in cellulose sheets

The degree of hygroscopic expansion of a porous sheet as the wetting front propagates is related to the amount of water absorbed in the sheet. See fig. S6 (section S4) for the schematic of the porous cellulose sheet being wetted. The hygroscopic strain $\varepsilon = \alpha\eta$, where α is the hygroscopic swelling coefficient measured to be $\alpha \approx 0.33$ (section S5 and fig. S7). The volume fraction of aqueous liquid, η, in the front sheet is given by $\eta = V_l / V_c$, with V_l and V_c being the volume of liquid and of cellulose, respectively. Because a liquid is absorbed into a sheet of thickness s by the distance l_d, $V_l \sim N_0 r_0 l_d s$. The diffusion length l_d is scaled as $l_d \sim (D\tau)^{1/2}$, with τ being the characteristic time taken for the rising liquid to pass the sheet: $\tau \sim s/u$. The diffusivity of a dense hygroscopic medium (19), D, is given by $D = 2Gk_c(1 - \nu)/(1 - 2\nu)/\mu$, where the shear modulus $G = 1.62$ MPa (section S6 and fig. S8), the permeability $k_c \sim r_c^2/32$, with r_c being the typical pore radius (order of 1 nm) of a cellulose sheet (25),

and Poisson's ratio $\nu = 0.3$ (26). The cellulose volume $V_c \sim N_0 r_0^2 s(1 - \phi)/\phi$, where the porosity ϕ is the ratio of the micropore volume to the total sheet volume (section S4 and fig. S6).

Although the moisture diffusion at the wetting front determines the size of newly wetted pores, the diffusion length itself is insignificant as compared with the overall rise height. Namely, we find that the typical increment of the diffusion length Δl_d is much smaller than that of the rise height Δh, to give $\Delta l_d/\Delta h \sim 0.01$ for a given duration even in the late stages.

Dynamics of wicking and swelling in late stages

The foregoing considerations allow us to write ε as $\varepsilon \sim \alpha(Ds/u)^{1/2}\phi/(1-\phi)/r_0$, which leads to

$$r \sim \left(\frac{\alpha\beta\phi r_0}{1 - \phi}\right)^{1/2} (Ds)^{1/4} u^{-1/4} \qquad (2)$$

The relation indicates that the micropore radius at the wet front increases as the liquid rising velocity (u) decreases, which results in the decrease in the capillary pressure ($\sim\gamma/r$). Combining Eqs. 1 and 2 and recalling $\dot{h} \approx u/\zeta$, we obtain a power law for the rise height in the late stages, $h \sim (Bt)^{1/5}$, with B given by

$$B = \frac{1}{\zeta} \left[\frac{\gamma^3(1 - \phi)^{1/2}}{\mu(\rho g)^2(\alpha\beta\phi r_0)^{1/2}(Ds)^{1/4}} \right]^{4/3} \qquad (3)$$

We plot the experimental results in the late stages of Fig. 4D according to scaling law (Eq. 3) in Fig. 4E. We see that the experimental data for various liquids are collapsed onto a single master curve despite the variations of γ, μ, ρ, and D, consistent with our theory. Figure 4F plots h based on the scaling law suggested for nonswelling sponges (13): $h \sim \{\gamma^3 t/[\mu(\rho g)^2 r_0]\}^{1/4}$. Although the data
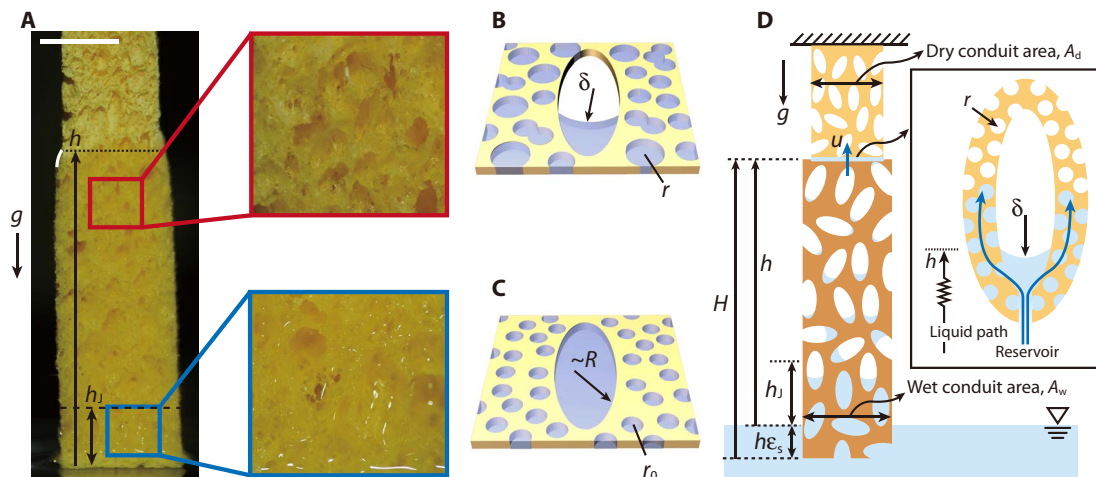
Fig. 3. The difference of wicking behavior between early and late stages. (**A**) Optical image of a sponge wetted by water. At small h, or in the early stages, the macro voids are completely filled with liquid. However, at large h, or in the late stages, they are only partially filled with liquid. A white curved line indicates the deformation of sponge due to the constraint of the dry upper part (section S1). The blue and red boxes show macro voids completely and partially filled with liquid, respectively. Scale bar, 10 mm. (**B**) Schematic of liquid-filling behavior in the late stages. Macro voids are not completely filled with liquid due to gravitational effects, whereas micropores are fully occupied with liquid. The radius of curvature δ of the meniscus in the macro void is determined by the balance between gravitational and capillary forces: $\delta \sim \gamma/(\rho g h)$. (**C**) Schematic of a macro void of radius R in a microporous sheet in the early stages. Both macro and micro voids are completely filled with liquid. (**D**) Simplified model of the sponge whose wetting behavior is mathematically analyzed. Black box shows the liquid path near the wetting front. The liquid permeates into micropores from the wet corner of macropores.
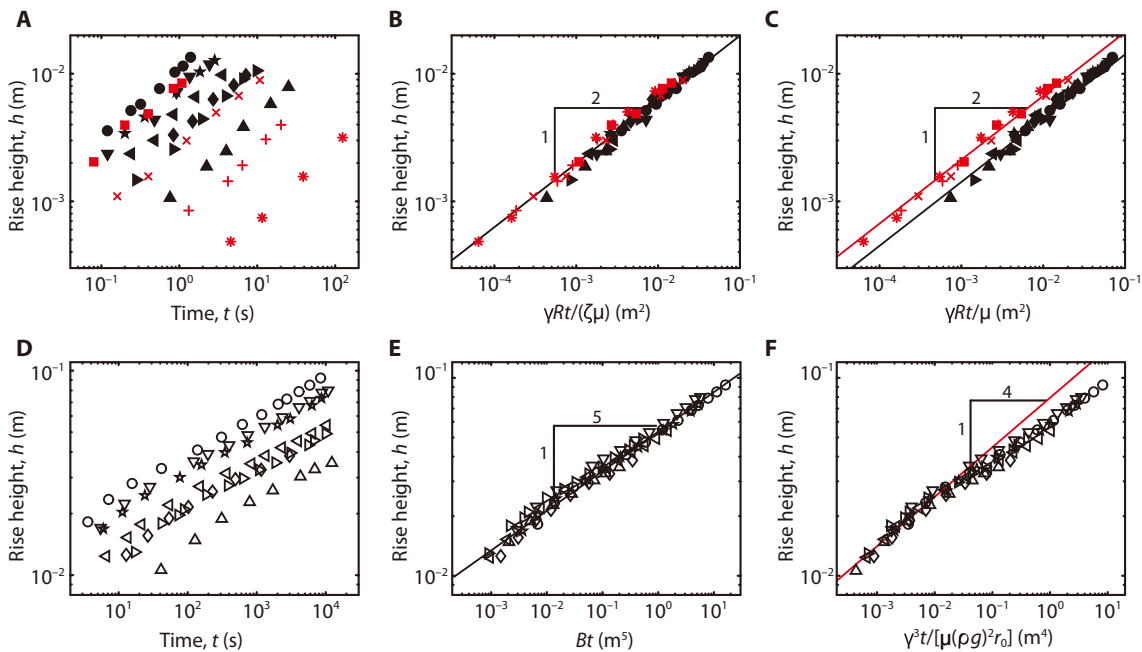

Fig. 4. Wicking dynamics in different stages. (**A**) Experimentally measured rise height versus time in the early stages. (**B**) The early-stage data are collapsed onto a single line when plotted according to our scaling law $h \sim [\gamma R t/(\zeta\mu)]^{1/2}$. The law holds for both the aqueous and nonaqueous liquids. (**C**) Two collapsed lines for aqueous (black line) and nonaqueous liquids (red line). (**D**) Experimentally measured rise height of aqueous liquids versus time in the late stages. (**E**) The late-stage data are collapsed onto a single line when plotted against our scaling law $h \sim (Bt)^{1/5}$. (**F**) The experimental results appear to collapse onto a single line but disobey the $t^{1/4}$ rule (Eq. 1). The symbols for different liquids are listed in table S1.

appear to collapse onto a single line, h does not follow $h \sim t^{1/4}$, invalidating the nonswelling theory for the current situation. We show in section S7 (fig. S9) that even with aqueous liquids, the rise height follows the $t^{1/4}$ law in the late stages for the sponges that have been pre-wetted and fully swollen in advance.

DISCUSSION

We have constructed the theoretical framework to analyze the liquid flow in hygroexpansive porous medium, where multiscale pore dynamics cannot be adequately accounted for by conventional poroelasticity theory. In particular, our analysis correctly captures the $t^{1/5}$ behavior of

the rise height in the late stages by considering the expansion of micropores as a function of the liquid rise speed, which determines the diffusion length within a cellulose sheet. Although the evaporation of water from the wet sponge occurs in the course of capillary rise, it has been ignored in our analysis because its rate ($q \approx 6 \times 10^{-9}$ m/s as experimentally measured) is negligibly small compared with the typical wicking velocity $u \sim 10^{-4}$ m/s in the late stages. We note that although cellulose is a major constituent of wood, the porous structure of artificially manufactured cellulose sponges is distinguished from wood that has grown in nature. One of those remarkable differences is that wood has submicrometric pores in a hierarchical order (25), which are invisible in the cellulose sponges.

Besides cellulose sponges, a variety of mundane and industrial materials of heterogeneous porosity can benefit from our theory, including biomedical devices such as the cytosponge (27), cell cultures (28), shape-morphing microneedles (29), soft actuators (30, 31), and plant seeds (32). Paper itself involves only microscale pores (33, 34), but crumpled or folded paper forms macro voids, wetting of which should be in line with the current problem. In addition to cellulosic porous materials, hygroexpansive porous bread composed of starch (35) was found to exhibit micropore coalescence and to follow the $t^{1/5}$ law in the late stages of vertical wicking (section S8 and fig. S10). This enables us to start thinking about applying our theoretical framework to a relevant field in the science of cooking. Although we have concentrated on the power-law behavior of liquid dynamics, hygroscopic deformation dynamics of the heterogeneous porous solid structure would help us to fully understand and control the soft materials of ever-growing importance.

MATERIALS AND METHODS
Experimental procedures of ESEM
In the ESEM chamber (XL-30 FEG, Philips), we placed a piece of cellulose sponge, $5 \times 5 \times 1$ mm^3 in volume, on a Peltier plate, which was kept at 2°C. Water vapor was supplied into the chamber to increase the RH. The sponge underwent drastic shape change as the environmental humidity reached approximately 90% by absorbing water molecules. The deformation of the sponge was insignificant when RH was below 90%, indicating that water molecules hardly infiltrate the sponge until the vapor pressure reaches a critical value. The imaging results are shown in Fig. 2D.

SUPPLEMENTARY MATERIALS
Supplementary material for this article is available at http://advances.sciencemag.org/cgi/content/full/4/3/eaao7051/DC1

section S1. Effects of isotropic volumetric expansion on liquid rise height
section S2. Correlation between hygroscopic strain and pore coalescence
section S3. Recovery of microporous structure of cellulose sponges
section S4. The volume fraction of aqueous liquid in a cellulose sheet
section S5. Effects of water concentration on hygroscopic strain
section S6. Mechanical properties of cellulose sponges
section S7. Capillary rise in pre-swollen sponges
section S8. Scaling laws of water rise within bread made from starch
fig. S1. The measurement data of the cellulose sponge structure.
fig. S2. Macroscopic experiments for pore coalescence.
fig. S3. Numerical analysis of porous sheet deformation.
fig. S4. Moisture flux into cellulose sheet in ESEM chamber.
fig. S5. Microporous structure of cellulose sponges after cycles of wetting and drying with water.
fig. S6. Analysis of the cellulose sheets.
fig. S7. Hygroscopic strain of saturated sponge for different water contents in aqueous glycerin and ethylene glycol.
fig. S8. Shear modulus of dry and wet cellulose sponge.
fig. S9. Capillary rise height of water versus time in an initially dry sponge (black) and pre-swollen sponge (red).
fig. S10. Capillary rise in porous bread.
table S1. List of liquid properties and symbols.
movie S1. Wicking and swelling in the cellulose sponge.
movie S2. The merging of micropores in the cellulose sheets.
References (36–38)

REFERENCES AND NOTES

1. R. C. Saxena, D. K. Adhikari, H. B. Goyal, Biomass-based energy fuel through biochemical routes: A review. *Renew. Sust. Energ. Rev.* **13**, 167–178 (2009).
2. M. A. García, C. Ferrero, N. Bértola, M. Martino, N. Zaritzky, Edible coatings from cellulose derivatives to reduce oil uptake in fried products. *Innov. Food Sci. Emerg. Technol.* **3**, 391–397 (2002).
3. J. F. Ang, Water retention capacity and viscosity effect of powdered cellulose. *J. Food Sci.* **56**, 1682–1684 (1991).
4. S. Goodhew, R. Griffiths, Sustainable earth walls to meet the building regulations. *Energ. Buildings* **37**, 451–459 (2005).
5. A. K. Bledzki, J. Gassan, Composites reinforced with cellulose based fibres. *Prog. Polym. Sci.* **24**, 221–274 (1999).
6. S. B. Stanković, D. Popović, G. B. Poparić, Thermal properties of textile fabrics made of natural and regenerated cellulose fibers. *Polym. Test.* **27**, 41–48 (2008).
7. P. C. K. Sankar, P. Ramakrishnan, M. J. Rosemary, Biological evaluation of nanosilver incorporated cellulose pulp for hygiene products. *Mater. Sci. Eng. C Mater. Biol. Appl.* **61**, 631–637 (2016).
8. Z. Weng, Y. Su, D.-W. Wang, F. Li, J. Du, H.-M. Cheng, Graphene–cellulose paper flexible supercapacitors. *Adv. Energy Mater.* **1**, 917–922 (2011).
9. M. Märtson, J. Viljanto, T. Hurme, P. Laippala, P. Saukko, Is cellulose sponge degradable or stable as implantation material? An in vivo subcutaneous study in rat. *Biomaterials* **20**, 1989–1995 (1999).
10. S. T. Nguyen, J. Feng, N. T. Le, A. T. T. Le, N. Hoang, V. B. C. Tan, H. M. Duong, Cellulose aerogel from paper waste for crude oil spill cleaning. *Ind. Eng. Chem. Res.* **52**, 18386–18391 (2013).
11. S. Capodicasa, S. Fedi, A. M. Porcelli, D. Zannoni, The microbial community dwelling on a biodeteriorated 16th century painting. *Int. Biodeter. Biodegr.* **64**, 727–733 (2010).
12. J. Kim, M.-W. Moon, K.-R. Lee, L. Mahadevan, H.-Y. Kim, Hydrodynamics of writing with ink. *Phys. Rev. Lett.* **107**, 264501 (2011).
13. J. Kim, J. Ha, H.-Y. Kim, Capillary rise of non-aqueous liquids in cellulose sponges. *J. Fluid Mech.* **818**, R2 (2017).
14. S. J. Kim, J. W. Choi, M.-W. Moon, K.-R. Lee, Y. S. Chang, D.-Y. Lee, H.-Y. Kim, Wicking and flooding of liquids on vertical porous sheets. *Phys. Fluids* **27**, 032105 (2015).
15. J. Kim, M.-W. Moon, H.-Y. Kim, Dynamics of hemiwicking. *J. Fluid Mech.* **800**, 57–71 (2016).
16. J. I. Siddique, D. M. Anderson, A. Bondarev, Capillary rise of a liquid into a deformable porous material. *Phys. Fluids* **21**, 013106 (2009).
17. M. A. Biot, General theory of three-dimensional consolidation. *J. Appl. Phys.* **12**, 155–164 (1941).
18. A. Nur, J. D. Byerlee, An exact effective stress law for elastic deformation of rock with fluids. *J. Geophys. Res.* **76**, 6414–6419 (1971).
19. J. Yoon, S. Cai, Z. Suo, R. C. Hayward, Poroelastic swelling kinetics of thin hydrogel layers: Comparison of theory and experiment. *Soft Matter* **6**, 6004–6012 (2010).
20. J. Jurin, An account of some experiments shown before the Royal Society; with an enquiry into the cause of the ascent and suspension of water in capillary tubes. *Philos. Trans.* **30**, 739–747 (1718).
21. R. Lucas, Ueber das Zeitgesetz des kapillaren Aufstiegs von Flüssigkeiten. *Kolloid Z.* **23**, 15–22 (1918).
22. E. W. Washburn, The dynamics of capillary flow. *Phys. Rev.* **17**, 273–283 (1921).
23. G. L. Roy, J. D. Embury, G. Edwards, M. F. Ashby, A model of ductile fracture based on the nucleation and growth of voids. *Acta Metall. Mater.* **29**, 1509–1522 (1981).
24. H. H. Kausch, Ph. Beguelin, M. Fischer, Failure of particulate reinforced polymers. *Mech. Compos. Mater.* **36**, 177–184 (2000).
25. D. Klemm, B. Heublein, H.-P. Fink, A. Bohn, Cellulose: Fascinating biopolymer and sustainable raw material. *Angew. Chem. Int. Ed. Engl.* **44**, 3358–3393 (2005).
26. R. J. Roberts, R. C. Rowe, P. York, The Poisson's ratio of microcrystalline cellulose. *Int. J. Pharm.* **105**, 177–180 (1994).
27. P. Lao-Sirieix, R. C. Fitzgerald, Screening for oesophageal cancer. *Nat. Rev. Clin. Oncol.* **9**, 278–287 (2012).
28. M. Bhattacharya, M. M. Malinen, P. Lauren, Y.-R. Lou, S. W. Kuisma, L. Kanninen, M. Lille, A. Corlu, C. GuGuen-Guillouzo, O. Ikkala, A. Laukkanen, A. Urtti, M. Yliperttula,

Nanofibrillar cellulose hydrogel promotes three-dimensional liver cell culture. *J. Control. Release* **164**, 291–298 (2012).

29. S. Y. Yang, E. D. O'Cearbhaill, G. C. Sisk, K. M. Park, W. K. Cho, M. Villiger, B. E. Bouma, B. Pomahac, J. M. Karp, A bio-inspired swellable microneedle adhesive for mechanical interlocking with tissue. *Nat. Commun.* **4**, 1702 (2013).

30. J. Y. Chung, H. King, L. Mahadevan, Evaporative microclimate driven hygrometers and hygromotors. *Europhys. Lett.* **107**, 64002 (2014).

31. A. S. Gladman, E. A. Matsumoto, R. G. Nuzzo, L. Mahadevan, J. A. Lewis, Biomimetic 4D printing. *Nat. Mater.* **15**, 413–418 (2016).

32. W. Jung, W. Kim, H.-Y. Kim, Self-burial mechanics of hygroscopically responsive awns. *Integr. Comp. Biol.* **54**, 1034–1042 (2014).

33. E. Reyssat, L. Mahadevan, Hygromorphs: From pine cones to biomimetic bilayers. *J. R. Soc. Interface* **6**, 951–957 (2009).

34. M. Lee, S. Kim, H.-Y. Kim, L. Mahadevan, Bending and buckling of wet paper. *Phys. Fluids* **28**, 042101 (2016).

35. N. N. Hellman, T. F. Boesch, E. H. Melvin, Starch granule swelling in water vapor sorption. *J. Am. Chem. Soc.* **74**, 348–350 (1952).

36. J. Kováčik, Correlation between Young's modulus and porosity in porous materials. *J. Mater. Sci. Lett.* **18**, 1007–1010 (1999).

37. Glycerine Producers' Association, *Physical Properties of Glycerine and Its Solutions* (Glycerine Producers' Association, 1963).

38. Y. S. Won, D. K. Chung, A. F. Mills, Density, viscosity, surface tension, and carbon dioxide solubility and diffusivity of methanol, ethanol, aqueous propanol, and aqueous ethylene glycol at 25°C. *J. Chem. Eng. Data* **26**, 140–141 (1981).

Citation: J. Ha, J. Kim, Y. Jung, G. Yun, D.-N. Kim, H.-Y. Kim, Poro-elasto-capillary wicking of cellulose sponges. *Sci. Adv.* **4**, eaao7051 (2018).